atoms

MDPI

Perspective

Diabatic Potential Energy Matrices at the Interface of Nonadiabatic Dynamics, Machine Learning, and Quantum Computing

Yuchen Wang

Department of Chemistry and James Franck Institute, University of Chicago, Chicago, IL 60637, USA; yuchenwang@uchicago.edu

Abstract

The accurate description of nonadiabatic quantum molecular dynamics represents one of the most significant challenges in modern computational chemistry, serving as a gateway to understanding complex phenomena ranging from photochemistry and electron transfer to surface scattering and biological exciton transport. A key difficulty lies in bridging high-level electronic structure theory for ground and excited states with accurate quantum dynamics theory. Although on-the-fly semiclassical approaches are increasingly viable, most quantum dynamics simulations still rely on pre-constructed potential energy surfaces, or in the nonadiabatic context, diabatic potential energy matrices (DPEMs). This perspective paper addresses the theoretical foundations, construction methodologies, and emerging frontiers of DPEMs. We examine the mathematical framework of the adiabatic-to-diabatic transformation, addressing the inherent topological challenges imposed by the geometric phase and the curl condition. We further analyze the transformative impact of machine learning, detailing how machine learning algorithms, such as permutation invariant polynomial neural networks and deep learning architectures, are reshaping the construction of global, high-dimensional DPEMs. Finally, we explore the disruptive potential of quantum computing, discussing how quantum algorithms are automating the direct simulation of nonadiabatic dynamics. In emerging quantum-centric workflows, DPEMs will continue to provide the critical bridge which enables the mapping of realistic, time-dependent molecular Hamiltonians onto quantum hardware.

Keywords: diabatic potential energy matrices; nonadiabatic molecular dynamics; conical intersections; machine learning; quantum computing; nonadiabatic coupling; neural networks; quantum simulation

Academic Editor: Pascal Quinet

Received: 3 February 2026
Revised: 1 March 2026
Accepted: 6 March 2026
Published: 8 March 2026

1. Introduction

The theoretical treatment of molecular systems has been dominated for nearly a century by the Born–Oppenheimer (BO) approximation [1]. By assuming that the motion of atomic nuclei ($M \sim 10^3$–10^5 a.u.) and electrons ($m_e = 1$ a.u.) can be separated due to their disparate masses, the BO approximation allows the electronic Schrödinger equation to be solved at fixed nuclear geometries. This yields the adiabatic potential energy surfaces (PESs) that form the conceptual landscape of modern chemistry. However, the adiabatic picture is fundamentally insufficient for describing processes such as photochemistry, charge transfer, and nonadiabatic atomic collisions and scattering. As molecules explore excited-state manifolds, they frequently encounter regions where electronic states become degenerate or quasi-degenerate, most notably at conical intersections (CIs) [2,3].

In the vicinity of a CI, the motion of electrons and nuclei become comparable, inducing a breakdown of the BO approximation. The nonadiabatic coupling term, a vector quantity involving the derivative of the electronic wave function, becomes singular at a CI, creating a cusp in the potential energy surface and rendering the nuclear Schrödinger equation numerically unstable. To circumvent this, the diabatic representation is introduced. Unlike adiabatic states, which are defined as eigenfunctions of the electronic Hamiltonian, diabatic states are constructed to vary smoothly as a function of nuclear geometry. In this representation, the singular kinetic energy coupling is transformed into smooth, off-diagonal potential energy coupling terms [4–6].

This perspective paper addresses the rapidly evolving field of diabatic potential construction, emphasizing the transition from manual, system-specific derivations to automated, data-driven workflows powered by machine learning and quantum computing.

1.1. The Nonadiabatic Couplings

The total molecular Hamiltonian H^T is partitioned into the nuclear kinetic energy operator T^{nuc} and the electronic Hamiltonian $H(r;R)$:

$$H^T(\mathbf{r},\mathbf{R}) = T^{nuc}(\mathbf{R}) + H(\mathbf{r};\mathbf{R}) = \sum_{\alpha=1}^{N_{nuc}} \frac{-1}{2M_\alpha}\nabla_\alpha^2 + H(\mathbf{r};\mathbf{R}) \tag{1}$$

where r and R denote the collective electronic and nuclear coordinates, respectively, and the semicolon indicates that their motion can be separated. N_{nuc} is the number of nuclei. In the adiabatic representation, the electronic wave functions satisfy the electronic Schrödinger equation,

$$H(\mathbf{r};\mathbf{R})\Psi_I(\mathbf{r};\mathbf{R}) = E_I(\mathbf{R})\Psi_I(\mathbf{r};\mathbf{R}), \tag{2}$$

where I labels the Ith electronic state. The nonadiabatic couplings arise from the action of ∇_α^2 on the parametric dependence of the total wave functions [2]. Below we will suppress the subscript α for simplicity. The dominant first-order interstate coupling, or simply the derivative coupling, is defined below as

$$\mathbf{f}^{IJ}(\mathbf{R}) = \langle \Psi_I(\mathbf{r};\mathbf{R})|\nabla|\Psi_J(\mathbf{r};\mathbf{R})\rangle_r \tag{3}$$

It is natural to expand $\Psi_I(r;R)$ in the basis of configuration state functions (CSFs) [7], where

$$\Psi_I(\mathbf{r};\mathbf{R}) = \sum_i^{N^{CSF}} c_i^I(\mathbf{R})\psi_i(\mathbf{r};\mathbf{R}). \tag{4}$$

Upon substituting Equation (4) into Equation (3), the derivative coupling separates into a configuration interaction (CI) contribution, computable within the CI expansion, and a CSF contribution, which is more subtle and originates from the coordinate dependence of the CSF basis

$$\mathbf{f}^{IJ}(\mathbf{R}) = \mathbf{f}^{IJ}_{(CSF)}(\mathbf{R}) + \mathbf{f}^{IJ}_{(CI)}(\mathbf{R}), \tag{5}$$

where

$$\mathbf{f}^{IJ}_{(CI)}(\mathbf{R}) = \langle \mathbf{c}_I(\mathbf{R})|\nabla|\mathbf{c}_J(\mathbf{R})\rangle_{\mathrm{CSF}} = \frac{1}{E_J - E_I}\langle \Psi_I(\mathbf{r};\mathbf{R})|\nabla\mathbf{H}(\mathbf{R})|\Psi_J(\mathbf{r};\mathbf{R})\rangle_{\mathrm{CSF}} \tag{6}$$

and

$$\mathbf{f}^{IJ}_{(CSF)}(\mathbf{R}) = \sum_{ij} c_i^I(\mathbf{R})\, c_j^J(\mathbf{R})\langle \psi_i(\mathbf{r};\mathbf{R})|\nabla|\psi_j(\mathbf{r};\mathbf{R})\rangle_r. \tag{7}$$

Note that the subscript CSF in Equation (6) indicates a dot product over the CSF space, and the subscript r in Equation (7) is a integration over electronic coordinates.

Since $\mathbf{f}^{IJ}_{(CI)}$ is inversely proportional to the adiabatic energy gap $\Delta E_{IJ}(R) = E_J(R) - E_I(R)$, as the system approaches a conical intersection where $\Delta E_{IJ} \to 0$, the coupling vector diverges ($\mathbf{f}^{IJ} \to \infty$). This singularity creates a cusp in the potential energy surface and renders the numerical propagation of wave functions unstable [2].

1.2. Adiabatic-to-Diabatic Transformation

To remove the singularity, we seek a unitary transformation $\mathbf{U}(\mathbf{R})$ that rotates the adiabatic basis $\{\Psi^a\}$ into a new, diabatic basis $\{\Psi^d\}$:

$$\mathbf{\Psi}^d(\mathbf{r};\mathbf{R}) = \mathbf{U}(\mathbf{R})\mathbf{\Psi}^a(\mathbf{r};\mathbf{R}) \tag{8}$$

Here superscripts a and d label adiabatic and diabatic representation, respectively. The defining condition for a *strictly diabatic* basis is that the derivative coupling vanishes identically in the new representation:

$$\mathbf{f}^d(\mathbf{R}) = \mathbf{U}(\mathbf{R})^\dagger \mathbf{f}^a(\mathbf{R})\mathbf{U}(\mathbf{R}) + \mathbf{U}^\dagger(\mathbf{R})\nabla\mathbf{U}(\mathbf{R}) = \mathbf{0}. \tag{9}$$

Rearranging this condition yields the fundamental first-order partial differential equation, known as the ADT equation [5]:

$$\nabla\mathbf{U}(\mathbf{R}) + \mathbf{f}^a(\mathbf{R})\mathbf{U}(\mathbf{R}) = 0. \tag{10}$$

The solution of this equation transforms the singular derivative couplings into smooth off-diagonal potential energy terms $V^d(\mathbf{R})$, allowing the diagonal diabatic potentials to cross smoothly at the CI seam. As a special case, for a two-state system, the transformation matrix $\mathbf{U}(\mathbf{R})$ is a planar rotation parameterized by a mixing angle $\theta(\mathbf{R})$.

1.3. Topological Constraints

While the ADT provides a formal resolution to the singularity problem, its existence is constrained by vector calculus. For the scalar field θ to be uniquely defined, the vector field must be conservative (irrotational). This leads to the *curl condition*:

$$\text{curl}\ \mathbf{f}^{IJ}(\mathbf{R}) = \frac{\partial f^{IJ}_\beta}{\partial R_\alpha} - \frac{\partial f^{IJ}_\alpha}{\partial R_\beta} = 0. \tag{11}$$

For diatomic molecules, the nuclear configuration space is one-dimensional, making the curl trivially zero; thus, strict diabatization is always possible. However, for polyatomic systems ($N \geq 3$), Mead and Truhlar proved that the nonadiabatic coupling field generally possesses a non-zero curl in the presence of a conical intersection [8]. This implies that a strictly diabatic basis does not exist globally for polyatomic systems. In practice, modern methods construct quasi-diabatic bases that remove the singular, longitudinal component of f_{IJ} while minimizing the residual transverse component of f_{IJ} [9,10]. Because the nuclear configuration space is a multi-dimensional manifold, the Hodge decomposition states that f_{IJ} cannot be exact, where the co-exact portion, which cannot be rotated away by a simple scalar gauge transformation, remains as the residual transverse component [11].

2. The Machine Learning Revolution in Diabatic Potentials

The integration of machine learning into chemical physics has fundamentally altered the landscape of potential energy surface construction. While machine learning regression of adiabatic, especially ground-state, potential energy surfaces has progressed rapidly, ML

models for full diabatic potential energy matrices (DPEMs) remain far less developed. This discrepancy arises from several challenges. First, it is straightforward to realize that a DPEM is an $N_s \times N_s$ electronic potential matrix for N_s states. Unlike a single PES, ML models must therefore output all diagonal energies and off-diagonal couplings of this matrix simultaneously, preserving its Hermitian symmetry. This multi-dimensional output requirement is more complex than fitting a single scalar surface. Moreover, two more profound reasons are listed below.

1. **Symmetry requirements:** Perhaps more important, and often misunderstood, is that unlike a single adiabatic PES, which is a scalar function and is automatically invariant under permutation of identical nuclei, a diabatic potential energy matrix must satisfy *covariant* symmetry constraints imposed by the complete nuclear permutation inversion (CNPI) group. Under a permutation of identical nuclei, the nuclear geometry is transformed and, simultaneously, the diabatic electronic basis may rotate within the multi-state subspace. As a result, the DPEM is required to transform as

$$\mathbf{V}(\hat{P}\mathbf{R}) = \mathbf{U}(\hat{P})\,\mathbf{V}(\mathbf{R})\,\mathbf{U}^{\dagger}(\hat{P}), \tag{12}$$

   where $\mathbf{U}(\hat{P})$ is a matrix representation of the CNPI operation in the diabatic state space. This requirement imposes nontrivial constraints on both diagonal energies and off-diagonal couplings, including possible sign changes or state mixing under permutation. In contrast, conventional PES fitting only enforces permutation invariance of a scalar quantity. Ensuring correct CNPI symmetry in a DPEM is essential for preserving nuclear indistinguishability, correct vibronic symmetry, and physically meaningful nonadiabatic dynamics, and substantially increases the difficulty of both analytic construction and machine learning-based fitting.
2. **Non-uniqueness of diabatic states:** Diabatic states and coupling elements are not directly provided by standard ab initio calculations and require a separate diabatization procedure. As a result, high-quality diabatic training data are scarce. The diabatic basis is not uniquely defined and may require arbitrary unitary rotations or phase conventions. Without additional constraints, ML fitting of the DPEM has infinitely many equivalent solutions when only adiabatic data are used, adding ambiguity. This lack of uniqueness and the need for extra constraints further complicates ML modeling of DPEMs.

Over the past two decades, ML has progressed from the regression of adiabatic potential energy surfaces toward the more rigorous construction of global diabatic Hamiltonian matrices [12–15]. This shift reflects the need to move beyond scalar energy fitting and address matrix-valued electronic structure objects that encode interstate couplings, symmetry constraints, and gauge freedom. In this section, we discuss the architectural innovations that allow ML models to respect exact physical symmetries, properly account for geometric phase effects, and remain scalable in high-dimensional nuclear configuration spaces.

2.1. Permutationally Invariant Polynomial Neural Networks (PIP-NN)

To accurately represent the high-dimensional landscapes of polyatomic systems, a diabatic matrix model must rigorously satisfy the symmetry constraints imposed by the CNPI group. The permutationally invariant polynomial neural network (PIP-NN) has emerged as a cornerstone methodology for this task, representing a synthesis of invariant theory and deep learning.

The foundation of the PIP-NN methodology lies in the seminal work of Braams and Bowman [16], who introduced the use of symmetrized monomials for fitting adiabatic potential energy surfaces. They demonstrated that internuclear distances r_{ij}, rather than

internal bond angles, provide a more robust basis for describing global surfaces, provided they are transformed into Morse-like variables to enforce asymptotic boundary conditions. While the initial approach relied on linear least-squares fitting of massive polynomial expansions, it suffered from the factorial scaling of the basis size with the number of atoms. Jiang and Guo [17] integrated these invariant polynomials as the input layer of a feed-forward neural network. This hybrid PIP-NN architecture leverages the network's ability to model complex non-linearities with a compact parameter set while guaranteeing exact permutational symmetry through the input features.

The construction of a PIP-NN for a diabatic potential energy matrix $\mathbf{V}^d(\mathbf{R})$ begins with the transformation of Cartesian coordinates $\mathbf{R}$ into variables including but not limited to Morse variables:

$$y_{ij} = \exp\left(-\frac{r_{ij}}{\lambda}\right) \tag{13}$$

where r_{ij} is the Euclidean distance between atoms i and j, and λ is a normalization parameter. The input vector $\mathbf{G} = \{G_1, G_2, \ldots, G_M\}$ for the neural network consists of permutationally invariant polynomials (PIPs), generated by applying a symmetrization operator $\hat{S}$ to the monomials:

$$G_k(\mathbf{y}) = \hat{S}\left[\prod_{i<j} y_{ij}^{n_{ij}^{(k)}}\right] = \frac{1}{|G|}\sum_{\hat{P}\in G_{CNPI}} \hat{P}\left[\prod_{i<j} y_{ij}^{n_{ij}^{(k)}}\right] \tag{14}$$

For a multi-state system, the diagonal elements $V_{ii}(\mathbf{R})$ are totally symmetric. However, the off-diagonal coupling elements $V_{ij}(\mathbf{R})$ $(i \neq j)$ must transform according to the direct product of the irreducible representations of the electronic states, $\Gamma_i \otimes \Gamma_j$. To enforce this, modern PIP-NNs employ a "diabatization by ansatz" approach, modeling the coupling as the product of a symmetry-carrying analytic function $f_{sym}(\mathbf{R})$ and a learned totally symmetric neural network output:

$$V_{ij}(\mathbf{R}) = f_{sym}(\mathbf{R}) \cdot \mathcal{N}_{ij}(\mathbf{G}) \tag{15}$$

This ensures that the nodal planes and phase changes required by the electronic symmetry are preserved across the entire nuclear configuration space [18].

The last few years have seen the maturation of PIP-NNs into a production-level tool for nonadiabatic dynamics. Some of the progresses includes:

1. **Fundamental invariants neural networks:** To bypass the computational bottleneck of generating thousands of symmetrized monomials for systems with >6 atoms, recent works have adopted fundamental invariants (FIs) [19,20]. FIs constitute a minimal generating set for the ring of invariants, allowing the input layer to remain compact and scalable for high-dimensional systems.
2. **Generalization to properties:** Yarkony and coworkers have pioneered the interpretation of molecular properties in nonadiabatic systems [18,21–24]. Unlike adiabatic energies which are continuous but not differentiable, the adiabatic molecular properties such as dipoles and spin–orbit couplings are fundamentally discontinuous in the adiabatic representation. Attempting to fit these irregular features directly with neural networks is error-prone. Instead, these works employ diabatization to transform the properties into a smooth, continuous representation that eliminates the singularities [18]. This rigorous treatment enables high-fidelity simulations of complex quantum phenomena, including intersystem crossing mechanisms [25,26] and light–matter interactions in cavity molecular dynamics [27,28].
3. **Reduced-information diabatization:** Recent studies have demonstrated that accurate DPEMs can be constructed using *only* adiabatic energies, bypassing the need for expensive nonadiabatic coupling vectors or derivative couplings [29–31]. By rigor-

ously enforcing the diabatic symmetry ansatz within the neural network architecture, the PIP-NN can essentially reverse-engineer the off-diagonal coupling terms. It infers the correct coupling topology solely from the specific shape of the avoided crossings and the potential energy gaps between adiabatic states. This approach significantly reduces the computational cost of generating the training set, as it requires only standard single-point energy calculations rather than complex wave function-based nonadiabatic coupling evaluations.

2.2. Novel ML Architectures and Their Potential Application in DPEMs

The last few years have witnessed great success in potential energy surface fitting. Examples include the phaseless corrections. As has been pointed out in Section 1.2, the sign of the adiabatic wave function $|\Psi_I\rangle$ is arbitrary and can flip randomly between geometries in a training set. This makes the nonadiabatic coupling vectors and off-diagonal DPEM elements discontinuous and unlearnable by smooth regression functions. Recent work has solidified clustering-based phase correction algorithms that use kernel ridge regression in an expectation-maximization loop to iteratively reassign signs to training data until a smooth surface is recovered [32].

The success of large language models has inspired transformer-type architectures for chemistry. One example is equivariant transformers (EqT) and message passing atomic cluster expansion (MACE), which replace standard scalar features with equivariant tensor products using Clebsch–Gordan coefficients to predict vector and tensor quantities directly [33]. In recent work [34], Zhu and Iyengar introduce a graph-based "LLM-type" architecture, where interacting molecular subsystems (nodes, edges, faces) are processed by a family of neural networks; this approach utilizes k-means tessellation for data efficiency and demonstrates remarkable transferability, enabling models trained on lower-dimensional systems to predict high-dimensional potential energy surfaces with sub-kcal/mol accuracy.

While the applications discussed here primarily target adiabatic chemistry and are not the central focus of this work, we anticipate that these methodologies can be naturally extended to nonadiabatic chemical processes in future studies. The main obstacles to such extensions arise from two fundamental challenges outlined above: the construction of quality diabatic representations and the faithful encoding of CNPI symmetry. For example, the use of the phaseless approximation, as commonly employed in auxiliary-field quantum Monte Carlo and related methods, may introduce systematic biases analogous to those observed in constrained-path or fixed-phase approximations. Understanding and mitigating these errors during the construction of DPEMs are necessary.

2.3. Highly Automatic Workflow of Diabatic Potential Energy Matrices

The construction of diabatic potential energy matrices (DPEMs) has historically been a "craft" rather than a routine calculation. Unlike many computational chemistry tools that are largely a black box, generating DPEMs requires making high-level choices regarding active spaces, diabatization methods, and phase consistency, which makes automatic workflow hard. However, recent literature highlights a shift toward fully automated, closed-loop workflows. This progress rests on several pillars.

1. **Automated Active Space Selection**: multi-configurational self-consistent field (MCSCF) is one of the most commonly used heuristics for nonadiabatic systems and also the starting point of many more advanced methods. Note that we exclude discussion of single-reference methods, as CIs exhibit multireference character, although remedies within single-reference frameworks have been proposed. However, MCSCF calculations are notoriously unstable and can converge to wrong roots or suffer from root-flipping during automated data generation. A "poisoned" data point

generated by a failed automated calculation can destroy the accuracy of the entire DPEM. The primary bottleneck in automating excited-state reference data is the selection of the active space for multiconfigurational calculations. A poor choice leads to intruder states and discontinuous surfaces. Recent protocols have successfully automated this decision processes such as AutoCAS. This algorithm utilizes density matrix renormalization group calculations to evaluate single-orbital entropies and mutual information. It automatically identifies the strongly correlated orbitals required for the active space based on quantum entanglement measures, removing user intuition from the loop [35,36].

2. **Active Learning and authomated diabatization**: Static grid sampling is inefficient for high-dimensional DPEMs. The field has shifted to a more active learning strategy. In this workflow, an ML model drives the dynamics, and uncertainty quantification triggers reference quantum calculations only when the model enters unexplored regions. Some examples include the MELTS framework [37]. Note that standard active learning is often insufficient for nonadiabatic systems because it may undersample the topologically complex regions near conical intersections. This has been addressed by, for example, gap-driven dynamics, a sampling strategy that specifically targets geometries with small adiabatic energy gaps, ensuring the automated workflow captures the seam where nonadiabatic couplings diverge [38].

Despite these advances, papers describing fully end-to-end black-box tools for DPEM construction remain scarce compared to ground-state potentials. Building a system that integrates unstable electronic structure theory, active learning dynamics, and neural network architectures requires a software stack that is difficult to maintain and distribute.

The future of automated DPEM construction lies in moving away from imposing physical ansatzes and toward learning the physics directly from data, such as in ansatz-free Hamiltonian learning. This would bypass the need for explicit diabatization ansatzes entirely. We anticipate a move toward generative models that can generate valid potential energy matrices conditioned on molecular graphs. By training models on massive databases of excited-state trajectories [39], it may be possible to predict approximate DPEMs for new molecules via transfer learning, drastically reducing the need for expensive ab initio data generation.

3. The Frontier of Quantum Computing for Nonadiabatic Dynamics

In Feynman's original formulation, a quantum computer is a computational framework for the efficient simulation of the probabilistic dynamics governing physical systems [40]. While machine learning has proven effective in accelerating the interpolation of potential energy surfaces, quantum computing offers the prospect of addressing the generation of electronic structure data itself, as well as enabling direct simulation of quantum dynamics. This capability is particularly compelling for strongly correlated and nonadiabatic systems, for which classical approaches encounter prohibitive exponential scaling.

There is growing recognition of a quantum-centric workflow in which quantum processors and classical high-performance computing (HPC) resources operate in tandem to enable the next generation of chemical simulations, as shown in Figure 1. Within this framework, DPEMs play a central bridging role, providing a compact and physically transparent representation that connects electronic structure theory with quantum dynamical propagation. In practice, DPEMs are constructed and validated on classical computers with the aid of machine learning and subsequently mapped onto quantum hardware, where they enable efficient simulation of nonadiabatic quantum dynamics beyond the reach of classical approaches.

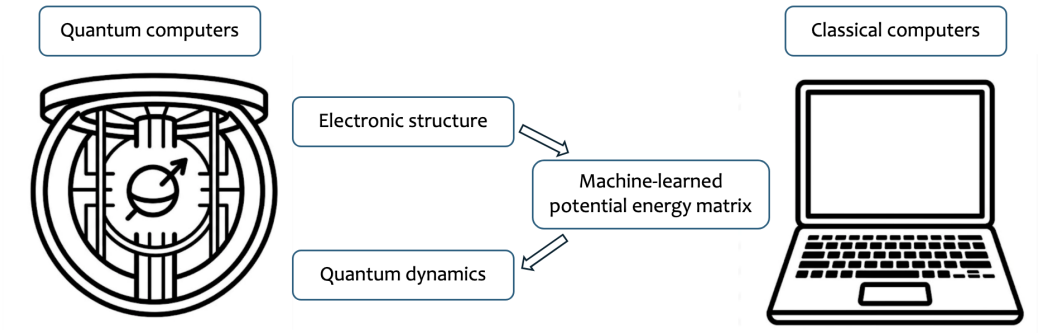

Figure 1. The proposed quantum–classical workflow for nonadiabatic quantum molecular dynamics.

3.1. Quantum Algorithms for Excited-State Electronic Structure

Due to the noisy nature of current quantum hardware, variational algorithms are the workhorses for chemical applications. Many methods have been developed to tackle the electronic structure of excited states. Variational quantum deflation (VQD) [41] finds excited states sequentially by minimizing a cost function that includes an orthogonality penalty to previously found states:

$$\mathcal{L}(\boldsymbol{\theta}_I) = \langle \Psi_I(\boldsymbol{\theta}_I)|\hat{H}|\Psi_I(\boldsymbol{\theta}_I)\rangle + \sum_{J=0}^{I-1} \beta_J \left|\langle \Psi_I(\boldsymbol{\theta}_I) \mid \Psi_J(\boldsymbol{\theta}_J)\rangle\right|^2. \tag{16}$$

Here, $\Psi_I(\boldsymbol{\theta}_I)$ denotes a parameterized variational approximation to the I-th electronic eigenstate of the Hamiltonian $\hat{H}$. Note the $(\mathbf{r};\mathbf{R})$ dependence is omitted for simplicity. $\boldsymbol{\theta}_I$ labels the variational parameters. The second term penalizes overlap with previously optimized lower-lying variational states $\{\Psi_J\}_{J<I}$. The penalty coefficients $\beta_J > 0$ control the strength of the orthogonality constraint and enforce approximate mutual orthogonality among the variationally obtained excited states.

Quantum computers offer a convenient way to implement unitary transformations acting simultaneously on sets of orthogonal states, since orthogonality is preserved under a common unitary operation [42,43]. This formulation can be viewed as an extension of the ensemble Rayleigh–Ritz variational principle. Recently, some progress has been made in nonadiabatic chemistry by exploring the conical intersection of cytosine with similar algorithms based on orthogonality [44].

Decent work has been made on the development of state-averaged orbital-optimized variational quantum eigensolver (SA-OO-VQE) quantum algorithm for nonadiabatic chemistry by Yalouz et al., where they established a rigorous framework for this approach by deriving analytical nonadiabatic couplings and gradients that account for orbital response, thereby enabling the precise simulation of molecular dynamics and the location of conical intersections [45]. On top of this, they introduced a method for the transformation-free generation of quasi-diabatic representations. By exploiting the intrinsic flexibility of the ansatz, this approach effectively circumvents the numerical instabilities associated with singular adiabatic-to-diabatic transformations, providing a robust means to characterize the topology of electronic degeneracies [46].

Alternative strategies to resolve the excited-state manifold include the use of spectral representations for variance-constrained targeting [47,48] and sample-based quantum diagonalization for efficient subspace projections [49]. Furthermore, the quantum Davidson method has been developed to iteratively expand Krylov subspaces, providing a robust route to low-lying states [50]. These varied methodologies collectively broaden the reach

of quantum computing for complex electronic spectra beyond state-averaging techniques, accounting for the possible non-orthogonality at conical intersections.

3.2. Quantum Dynamics on Quantum Computers

Beyond static potentials, quantum computers can simulate time evolution, $\hat{U}(t) = e^{-i\hat{H}t}$, directly. The standard approach is Trotterization, which decomposes the exponential into a product of non-commuting terms:

$$e^{-i\hat{H}t} \approx \left(\prod_k e^{-i\hat{H}_k \Delta t} \right)^{t/\Delta t}. \tag{17}$$

By mapping the molecular Hamiltonian across nuclear geometries, these time-evolution operators can be integrated into ab initio nonadiabatic molecular dynamics schemes to propagate electronic wave packets. This framework allows for the direct simulation of population transfers and coherences without the scaling bottlenecks of classical algorithms.

The emerging frontier of nonadiabatic dynamics focuses on the behavior of molecular systems within open quantum environments [51]. Accounting for environmental dissipation and decoherence is essential for accurately modeling chemical processes in the condensed phase or within optical cavities. Future research in this domain aims to leverage open-system quantum algorithms to capture the complex interplay between electronic transitions and bath-induced relaxation.

Another validation of nonadiabatic theory has come from analog quantum simulations [52,53]. In a series of landmark experiments [52], trapped-ion devices were designed to simulate a conical intersection. They mapped the electronic states to the ion's internal hyperfine levels and the nuclear coordinates to the physical motion. By driving the ion with state-dependent optical forces, they synthesized a model Hamiltonian and allowed for the direct observation of the geometric phase. As the wave packet encircled the CI point in parameter space, interferometry revealed the predicted π phase shift, a fundamental topological feature that had eluded direct observation in molecular experiments.

3.3. DPEM: Bridging Electronic Structure Theory with Quantum Dynamics

While the previously reviewed article establishes foundational principles for quantum simulations of nonadiabatic dynamics, the Hamiltonians considered therein are predominantly synthesized or toy Hamiltonians. Although such constructions successfully capture essential physical phenomena, they remain idealized representations. From a chemist's perspective, a central objective is to extend these approaches to realistic molecular systems, where quantitative accuracy and predictive power are essential.

In practical quantum molecular dynamics, for example within grid-based quantum simulation frameworks, the availability of high-quality DPEMs is a critical prerequisite. These DPEMs must accurately represent both the potential energy surfaces and the associated couplings across relevant regions of nuclear configuration space. Constructing such representations typically requires extensive ab initio electronic structure calculations, followed by careful fitting procedures to ensure smoothness, symmetry preservation, and correct asymptotic behavior. As system size and electronic complexity increase, especially in strongly correlated or near-degenerate regimes, the cost and difficulty of generating reliable DPEMs can become prohibitive. Bridging this gap will require systematic strategies for integrating high-fidelity electronic structure data with quantum simulation protocols, as well as scalable methods for diabatization and Hamiltonian construction that remain tractable beyond low-dimensional or weakly correlated systems.

4. Discussion and Future Outlook

We anticipate an emerging paradigm in which quantum simulation and machine learning are combined into a tightly integrated hybrid quantum–classical–AI workflow. Rather than viewing quantum computers as standalone replacements for classical computers, their near- and mid-term utility lies in their selective deployment at points of maximal theoretical and computational difficulty, coupled to data-efficient learning and direct dynamical propagation.

Within this framework, quantum hardware is primarily tasked with data generation at chemically and physically critical configurations and the high-fidelity propagation of electronic wave packets. Importantly, this usage pattern minimizes quantum resource requirements by restricting quantum calculations to sparse, high-impact regions of configuration space or specific time-evolution windows that defy classical approximation. The resulting quantum data can be incorporated into AI-driven diabatization pipelines. A critical component of this workflow is active learning. Once the diabatic representation is learned, the quantum processor can be deployed to propagate the nonadiabatic wave packet directly. By utilizing Trotterized evolution or variational algorithms, the quantum computer handles the coherent transitions at nonadiabatic seams, providing a rigorous alternative to classical devices.

While significant challenges remain in hardware scaling, the convergence of these approaches suggests a realistic route toward quantitatively reliable nonadiabatic simulations. Rather than eliminating the nonadiabatic problem, this hybrid paradigm reframes it as an engineering challenge, guided by the informed deployment of quantum resources for both representation and evolution.

Finally, the treatment of dissipative and environmental effects represents a critical frontier where quantum simulations can extend the reach of traditional nonadiabatic models. By leveraging ancilla-assisted or noise-resilient algorithms to simulate open quantum systems, one can rigorously capture the decoherence and relaxation pathways that define nonadiabatic molecular behavior.

Funding: This research received no external funding.

Data Availability Statement: No new data were created or analyzed in this study. Data sharing is not applicable to this article.

Conflicts of Interest: The author declares no conflicts of interest.

References

1. Born, M.; Oppenheimer, R. Zur Quantentheorie der Molekeln. *Ann. Phys.* **1927**, *389*, 457–484. [CrossRef]
2. Yarkony, D.R. Diabolical conical intersections. *Rev. Mod. Phys.* **1996**, *68*, 985–1013. [CrossRef]
3. Domcke, W.; Yarkony, D.R.; Köppel, H. *Conical Intersections: Electronic Structure, Dynamics and Spectroscopy*; World Scientific: Singapore, 2004.
4. Smith, F.T. Diabatic and adiabatic representations for atomic collision problems. *Phys. Rev.* **1969**, *179*, 111–123. [CrossRef]
5. Baer, M. *Beyond Born–Oppenheimer: Electronic Nonadiabatic Coupling Terms and Conical Intersections*; Wiley: Hoboken, NJ, USA, 2006.
6. Yarkony, D.R.; Xie, C.; Zhu, X.; Wang, Y.; Malbon, C.L.; Guo, H. Diabatic and adiabatic representations: Electronic structure caveats. *Comput. Theor. Chem.* **2019**, *1152*, 41–50. [CrossRef]
7. Shavitt, I. The method of configuration interaction. In *Methods of Electronic Structure Theory*; Springer: Berlin/Heidelberg, Germany, 1977; pp. 189–275.
8. Mead, C.A.; Truhlar, D.G. Conditions for the definition of a strictly diabatic electronic basis for molecular systems. *J. Chem. Phys.* **1982**, *77*, 6090–6098. [CrossRef]
9. Xie, C.; Malbon, C.L.; Guo, H.; Yarkony, D.R. Up to a sign. The insidious effects of energetically inaccessible conical intersections on unimolecular reactions. *Acc. Chem. Res.* **2019**, *52*, 501–509. [CrossRef]
10. Wang, Y.; Xie, C.; Guo, H.; Yarkony, D.R. A quasi-diabatic representation of the $1,2^1$A states of methylamine. *J. Phys. Chem. A* **2019**, *123*, 5231–5241. [CrossRef]

11. Nakahara, M. *Geometry, Topology and Physics*; CRC Press: Boca Raton, FL, USA, 2018.
12. Cigrang, L.L.; Curchod, B.F.; Ingle, R.A.; Kelly, A.; Mannouch, J.R.; Accomasso, D.; Alijah, A.; Barbatti, M.; Chebbi, W.; Doslic, N.; et al. Roadmap for molecular benchmarks in nonadiabatic dynamics. *J. Phys. Chem. A* **2025**, *129*, 7023–7050. [CrossRef] [PubMed]
13. Westermayr, J.; Gastegger, M.; Menger, M.F.; Mai, S.; González, L.; Marquetand, P. Machine learning enables long time scale molecular photodynamics simulations. *Chem. Sci.* **2019**, *10*, 8100–8107. [CrossRef]
14. Müller, C.; Sršeň, Š.; Bachmair, B.; Crespo-Otero, R.; Li, J.; Mausenberger, S.; Pinheiro, M.; Worth, G.; Lopez, S.A.; Westermayr, J. Machine learning for nonadiabatic molecular dynamics: Best practices and recent progress. *Chem. Sci.* **2025**, *16*, 17542–17567. [CrossRef]
15. Richings, G.W.; Polyak, I.; Spinlove, K.E.; Worth, G.A.; Burghardt, I.; Lasorne, B. Quantum dynamics simulations using Gaussian wavepackets: The vMCG method. *Int. Rev. Phys. Chem.* **2015**, *34*, 269–308. [CrossRef]
16. Braams, B.J.; Bowman, J.M. Permutationally invariant potential energy surfaces in high dimensionality. *Int. J. Quantum Chem.* **2009**, *109*, 3178–3200. [CrossRef]
17. Jiang, B.; Guo, H. Permutation invariant polynomial neural network approach to fitting potential energy surfaces. *J. Chem. Phys.* **2013**, *139*, 054112. [CrossRef]
18. Wang, Y.; Guan, Y.; Guo, H.; Yarkony, D.R. Enabling complete multichannel nonadiabatic dynamics: A global representation of the two-channel coupled $1,2^1$A and 1^3A states of NH_3 using neural networks. *J. Chem. Phys.* **2021**, *154*, 094121. [CrossRef]
19. Shao, K.; Chen, J.; Zhao, Z.; Zhang, D.H. Communication: Fitting potential energy surfaces with fundamental invariant neural network. *J. Chem. Phys.* **2016**, *145*, 071101. [CrossRef]
20. Chen, R.; Shao, K.; Fu, B.; Zhang, D.H. Fitting potential energy surfaces with fundamental invariant neural network. II. Generating fundamental invariants for molecular systems with up to ten atoms. *J. Chem. Phys.* **2020**, *152*, 204307. [CrossRef]
21. Wang, Y.; Yarkony, D.R. Determining whether diabolical singularities limit the accuracy of molecular property based diabatic representations: The $1,2^1$A states of methylamine. *J. Chem. Phys.* **2018**, *149*, 154108. [CrossRef] [PubMed]
22. Wang, Y.; Guan, Y.; Yarkony, D.R. On the impact of singularities in the two-state adiabatic to diabatic state transformation: A global treatment. *J. Phys. Chem. A* **2019**, *123*, 9874–9885. [CrossRef] [PubMed]
23. Han, S.; Wang, Y.; Guan, Y.; Yarkony, D.R.; Guo, H. Impact of diabolical singular points on nonadiabatic dynamics and a remedy: Photodissociation of ammonia in the first band. *J. Chem. Theory Comput.* **2020**, *16*, 6776–6788. [CrossRef] [PubMed]
24. Wang, Y.; Yarkony, D.R. Conical intersection seams in spin-orbit coupled systems with an even number of electrons: A numerical study based on neural network fit surfaces. *J. Chem. Phys.* **2021**, *155*, 174115. [CrossRef]
25. Wang, Y.; Guo, H.; Yarkony, D.R. Internal conversion and intersystem crossing dynamics based on coupled potential energy surfaces with full geometry-dependent spin–orbit and derivative couplings: Nonadiabatic photodissociation dynamics of NH_3 A leading to the NH($a^1\Delta$, $X^3\Sigma^-$) + H_2 channel. *Phys. Chem. Chem. Phys.* **2022**, *24*, 15060–15072. [CrossRef] [PubMed]
26. Bachmair, B.; Dietschreit, J.C.; González, L. Revisiting the intricate photodissociation mechanism of ammonia along the minor NH + H_2 pathway. *Phys. Chem. Chem. Phys.* **2025**, *27*, 8212–8220. [CrossRef]
27. Avanessian, C.; Wang, Y.; Yarkony, D.R. Floquet-engineered photodissociation simulated using coupled potential energy and dipole matrices. *J. Phys. Chem. Lett.* **2024**, *15*, 9905–9912. [CrossRef]
28. Avanessian, C. Intersystem crossing in the molecular channel of ammonia photodissociation manipulated by an external laser field. *J. Chem. Phys.* **2025**, *163*, 084311. [CrossRef] [PubMed]
29. Lenzen, T.; Manthe, U. Neural network based coupled diabatic potential energy surfaces for reactive scattering. *J. Chem. Phys.* **2017**, *147*, 084105. [CrossRef]
30. Li, C.; Hou, S.; Xie, C. Constructing diabatic potential energy matrices with neural networks based on adiabatic energies and physical considerations: Toward quantum dynamic accuracy. *J. Chem. Theory Comput.* **2023**, *19*, 3063–3079. [CrossRef] [PubMed]
31. Hou, S.; Wang, Z.; Xie, C. Accurate and Efficient Schemes for Mapping Out Two Isolated Seams of Conical Intersections with Neural Networks Solely Based on Adiabatic Energies: A Case Study of H^+ + NO ($X^2\Pi$)→ H + NO^+ ($X^1\Sigma^+$). *J. Phys. Chem. A* **2024**, *128*, 7046–7054. [CrossRef]
32. Shu, Y.; Kryven, J.; Sampaio de Oliveira-Filho, A.G.; Zhang, L.; Song, G.L.; Li, S.L.; Meana-Pañeda, R.; Fu, B.; Bowman, J.M.; Truhlar, D.G. Direct diabatization and analytic representation of coupled potential energy surfaces and couplings for the reactive quenching of the excited $^2\Sigma^+$ state of OH by molecular hydrogen. *J. Chem. Phys.* **2019**, *151*, 104311. [CrossRef]
33. Batatia, I.; Kovacs, D.P.; Simm, G.; Ortner, C.; Csányi, G. MACE: Higher order equivariant message passing neural networks for fast and accurate force fields. *Adv. Neural Inf. Process. Syst.* **2022**, *35*, 11423–11436.
34. Zhu, X.; Iyengar, S.S. Large Language Model-Type Architecture for High-Dimensional Molecular Potential Energy Surfaces. *Phys. Rev. X* **2026**, *16*, 011012. [CrossRef]
35. Stein, C.J.; Reiher, M. autoCAS: A program for fully automated multiconfigurational calculations. *J. Comput. Chem.* **2019**, *40*, 2216–2226. [CrossRef] [PubMed]
36. Sayfutyarova, E.R.; Sun, Q.; Chan, G.K.L.; Knizia, G. Automated construction of molecular active spaces from atomic valence orbitals. *J. Chem. Theory Comput.* **2017**, *13*, 4063–4078. [CrossRef] [PubMed]

37. Bispo, M.d.O.; Souza Mattos, R.; Pinheiro, M., Jr.; Garain, B.C.; Dral, P.O.; Barbatti, M. MELTS: Fully Automated Active Learning for Fewest-Switches Surface Hopping Dynamics. *J. Chem. Theory Comput.* **2025**, *21*, 11390–11400. [CrossRef]
38. Martyka, M.; Zhang, L.; Ge, F.; Hou, Y.F.; Jankowska, J.; Barbatti, M.; Dral, P.O. Charting electronic-state manifolds across molecules with multi-state learning and gap-driven dynamics via efficient and robust active learning. *npj Comput. Mater.* **2025**, *11*, 132. [CrossRef]
39. Curth, R.; Röhrkasten, T.E.; Müller, C.; Westermayr, J. Surface Hopping Nested Instances Training Set for Excited-state Learning. *Sci. Data* **2025**, *12*, 1300. [CrossRef]
40. Feynman, R.P. Simulating Physics with Computers. *Int. J. Theor. Phys.* **1982**, *21*, 467–488. [CrossRef]
41. Higgott, O.; Wang, D.; Brierley, S. Variational Quantum Deflation: The spectrum of difference. *Quantum* **2019**, *3*, 156. [CrossRef]
42. Benavides-Riveros, C.L.; Wang, Y.; Warren, S.; Mazziotti, D.A. Quantum simulation of excited states from parallel contracted quantum eigensolvers. *New J. Phys.* **2024**, *26*, 033020. [CrossRef]
43. Dutta, R.; Cianci, C.; Soudackov, A.V.; Wang, Y.; Xu, C.; Mazziotti, D.A.; Santos, L.F.; Batista, V.S. Qumode-Based Variational Quantum Eigensolver for Molecular Excited States. *J. Chem. Theory Comput.* **2026**, *22*, 993–1003. [CrossRef]
44. Wang, Y.; Cianci, C.; Avdic, I.; Dutta, R.; Warren, S.; Allen, B.; Vu, N.P.; Santos, L.F.; Batista, V.S.; Mazziotti, D.A. Characterizing conical intersections of nucleobases on quantum computers. *J. Chem. Theory Comput.* **2025**, *21*, 1213–1221. [CrossRef]
45. Yalouz, S.; Koridon, E.; Senjean, B.; Lasorne, B.; Buda, F.; Visscher, L. Analytical nonadiabatic couplings and gradients within the state-averaged orbital-optimized variational quantum eigensolver. *J. Chem. Theory Comput.* **2022**, *18*, 776–794. [CrossRef]
46. Illésová, S.; Beseda, M.; Yalouz, S.; Lasorne, B.; Senjean, B. Transformation-free generation of a quasi-diabatic representation from the state-average orbital-optimized variational quantum eigensolver. *J. Chem. Theory Comput.* **2025**, *21*, 5457–5480. [CrossRef]
47. Wang, Y.; Mazziotti, D.A. Electronic excited states from a variance-based contracted quantum eigensolver. *Phys. Rev. A* **2023**, *108*, 022814. [CrossRef]
48. Wang, Y.; Mazziotti, D.A. Quantum simulation of conical intersections. *Phys. Chem. Chem. Phys.* **2024**, *26*, 11491–11500. [CrossRef]
49. Barison, S.; Moreno, J.R.; Motta, M. Quantum-centric computation of molecular excited states with extended sample-based quantum diagonalization. *Quantum Sci. Technol.* **2025**, *10*, 025034. [CrossRef]
50. Tkachenko, N.V.; Cincio, L.; Boldyrev, A.I.; Tretiak, S.; Dub, P.A.; Zhang, Y. Quantum Davidson algorithm for excited states. *Quantum Sci. Technol.* **2024**, *9*, 035012. [CrossRef]
51. Delgado-Granados, L.H.; Krogmeier, T.J.; Sager-Smith, L.M.; Avdic, I.; Hu, Z.; Sajjan, M.; Abbasi, M.; Smart, S.E.; Narang, P.; Kais, S.; et al. Quantum algorithms and applications for open quantum systems. *Chem. Rev.* **2025**, *125*, 1823–1839. [CrossRef]
52. Whitlow, J.; Jia, Z.; Wang, Y.; Fang, C.; Kim, J.; Brown, K.R. Quantum simulation of conical intersections using trapped ions. *Nat. Chem.* **2023**, *15*, 1509–1514. [CrossRef] [PubMed]
53. Valahu, C.H.; Olaya-Agudelo, V.C.; MacDonell, R.J.; Navickas, T.; Rao, A.D.; Millican, M.J.; Pérez-Sánchez, J.B.; Yuen-Zhou, J.; Biercuk, M.J.; Hempel, C.; et al. Direct observation of geometric-phase interference in dynamics around a conical intersection. *Nat. Chem.* **2023**, *15*, 1503–1508. [CrossRef]